ELSEVIER

Polymer 41 (2000) 4881–4887

polymer

Factors affecting the limiting crack velocity in polymeric materials

J.P. Dear*

Department of Mechanical Engineering, Imperial College of Science, Technology and Medicine, Exhibition Road, London SW7 2BX, UK

Received 3 June 1999; received in revised form 24 August 1999; accepted 29 September 1999

Abstract

It is often stated that the theoretical limit for the velocity of crack propagation in materials relates to the free surface Rayleigh wave velocity or other wave related criteria [Roberts DK, Wells AA. Engineering 1954;171:820; Field JE. Contemporary Physics, 1983;24(5):439; Schardin H. In: Averbach BL, Fellbeck DJK, Hahn GT, Thomas DA, editors. Fracture, chap. 16, New York: Wiley, 1959; Anderson OL. In: Averbach BL, Fellbeck DJK, Hahn GT, Thomas DA, editors. Fracture, chap. 17, New York: Wiley, 1959.] However, the limiting crack velocity in many materials is less than this theoretical limit and considerably so for tough polymers. Using experimental fracture data obtained from a range of tough polymers, and a computer model in which toughness, stiffness and other material parameters can be independently varied, relationships have been identified between limiting crack velocity and toughness properties of polymers.

Keywords: Limiting crack velocity; Polymers; Modelling

1. Introduction

Loss of integrity in stressed products and structures can be life threatening and costly in many ways. This threat can be presented by extending cracks and fast cracks give little warning of what can be catastrophic failures. Key fracture data needed are the threshold load that will just maintain crack propagation, and the increase of crack velocity with load up to the limiting crack velocity condition. To obtain constant crack velocity in a specimen for each applied load, the material needs to be of consistent quality and dimensions. This is to obtain an even distribution of stress that can be particularly difficult to achieve in large specimens. A problem with small specimens is that it can be difficult to isolate crack initiation from crack propagation. However, for polymeric materials, this is possible using the frozen tongue technique [1]. With the size of specimen used in the frozen tongue experiments, the whole crack path can be closely monitored. This is to measure crack velocity, the rise and fall of stress at the crack tip, and obtain other data including the effect of stress relaxation in the material [1,2].

With these experimental studies, it was helpful to have a computer model that could represent the dynamic behaviour of materials examined. This was so that the toughness, stiffness and other material parameters could be changed independently to study their effect on the dynamic fracture behaviour of materials. Dynamic finite element models are very useful for this purpose, but reconfiguring them for many different studies is time-consuming. For this study, a distributed mass-spring model [3] was used, which had the advantage that the dynamic processes, represented by the model, were easy to visualise. This good visibility was most helpful when studying the effect of changing the modulus, Poisson's ratio and the crack path toughness of the materials simulated. The model provided was for studying self-propagating cracks, but for this study it was operated in the generation mode to obtain dynamic energy release rates for many different crack velocities. Another advantage of the distributed mass-spring model, for this study, is that it could be hosted on the same modest-sized PC used to capture and process experimental data.

The combined data from the frozen tongue experiments, and the distributed mass-spring model usefully provides for predictions to be made about new materials to be developed. It is to be noted that the inherent fracture properties of the materials studied, under steady state load conditions, have many uses. For example, it shows that for brittle materials, only a small additional load above that to just maintain crack propagation will result in a crack velocity close to the limiting condition. The steady state fracture data is therefore useful in analysing impact and other fracture properties of materials. A great deal of materials research

* Tel.: +44-0171-594-7086; fax: +44-0171-823-8845.
E-mail address: j.dear@ic.ac.uk (J.P. Dear).

0032-3861/00/$ - see front matter
PII: S0032-3861(99)00715-6

is devoted to achieving a high threshold load for crack propagation in the material and a low limiting crack velocity. However, the material also needs to have appropriate stiffness and other properties for each application.

In common with most finite element models, the distributed mass-spring model computations relate to a single toughness parameter which represents the many energy absorbing fracture processes at and about the propagating crack tip, including yielding, crazing, micro-cracking, drawing of fibrils and hot-spots. This is acceptable for homogeneous polymers, particularly the tougher polymers. However, for some brittle materials that have, for example, planes of weakness, more detailed experimentation and modelling is needed. Researchers [4–6] have reported that crack velocities in excess of the Rayleigh wave velocity are possible in these brittle materials and their toughness can relate mainly to cleavage, bifurcation or other specific fracture processes.

2. Frozen tongue experimental procedure

In this study, rectangular specimens of exactly the same size and shape were obtained for the following materials: styrene–acrylonitrile (SAN), polycarbonate (PC), three different grades of polyethylene (PE1, PE2 and PE3 in order of increasing toughness) and acrylonitrile–butadiene–styrene (ABS). These rectangular specimens were provided with a small tongue extension, at the beginning of the crack path, so that the frozen tongue technique [1,2] could be used to fracture the material. The specimens were side-grooved to minimise side-lip tearing so as to achieve, in the centre of the fracture surfaces, as near to plane strain conditions as possible. For each material, crack velocity versus applied load curves were obtained, under steady state fracture conditions, from the threshold load for crack propagation up to the limiting crack velocity condition.

The frozen tongue technique takes advantage of the good thermal insulation properties of polymers which permits a small tongue of material, at the beginning of the crack path, to be freeze-cooled with liquid nitrogen, so that a crack can be easily initiated in the tongue with a low force device. The freezing of the tongue and the application of the crack initiation force were confined to the half of the tongue furthest from the main section of the specimen. It was verified that this crack initiation procedure only caused a very small change in the stress and temperature for the first 5% of the crack path in the main section of the specimen [1]. It was possible, in a series of experiments, each with different loading of the main section, to determine the threshold load which would just maintain crack propagation in the material, and also how crack velocity varied with increasing load up to the limiting condition. Fig. 1 illustrates the frozen tongue technique, including the three-point bend method for starting a sharp crack in the frozen tongue. The dimensions of the stressed main section for the frozen tongue specimens

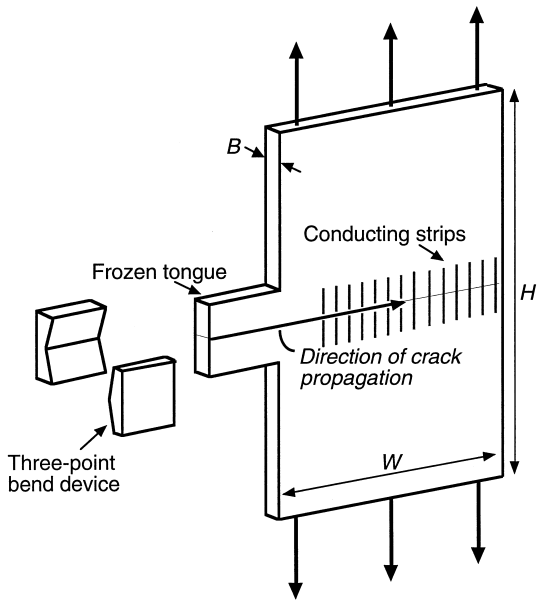

Fig. 1. Frozen tongue specimen geometry. The width (W) of the main section of the specimen is 90 mm, the height (H) of the stressed main section is 180 mm and the thickness (B) is 6 mm. The tongue is 40 mm by 40 mm. The three-point bend device for crack initiation of the tongue is also shown.

were: width $(W) = 90$ mm, height $(H) = 180$ mm and thickness $(B) = 6$ mm. The dimensions of the tongue section of the specimen were 40 mm by 40 mm. Side grooves of depth 1 mm were used on all the specimens to provide for near to plane-strain fracture conditions. Prior to crack initiation, the main section of the frozen tongue specimen was loaded at a constant strain rate of 5 mm min^{-1}, using an Instron tensile loading machine. At the required load, the machine cross-head was stopped and the specimen allowed to stress relax. After cooling of the tongue, a crack was then initiated using the low-force, static three-point bend loading device. For each loading level of the main section, crack velocity was measured using a combination of high-speed photography and on-specimen instrumentation. For the latter, a series of conducting strips were painted onto the specimen across the line of the crack path. As these strips were broken, a staircase voltage output from an electrical circuit gave crack length versus time and hence crack velocity. This was confirmed using high-speed photography (image converter IMACON 468 camera) with backlighting so that the crack appeared as a bright streak of light passing through the specimen. The breaking of the first conducting strip triggered the camera.

3. Distributed mass-spring model

The model comprised of a distributed mass-spring network as illustrated in Fig. 2. Only one half of the single edge-notch frozen tongue specimen was modelled as shown,

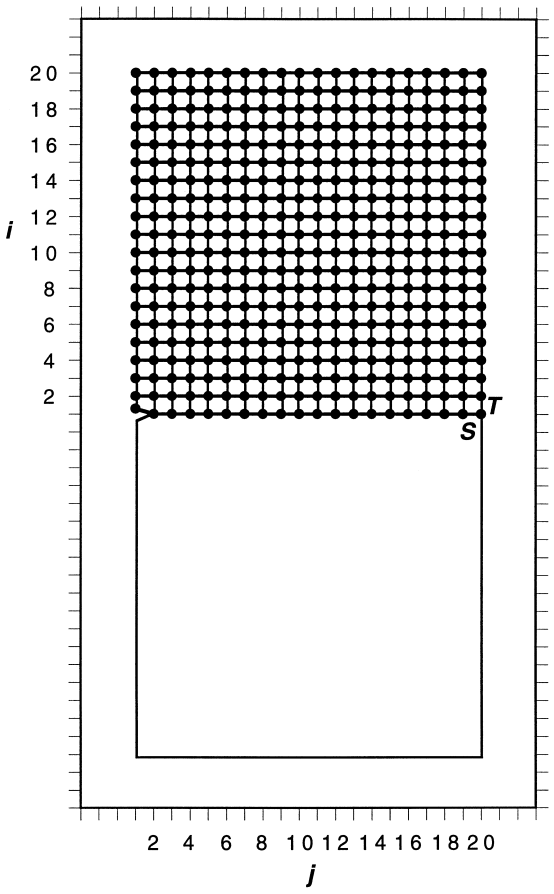

Fig. 2. Distributed mass-spring network showing initial displacements of masses, tension (T) and shear (S) spring elements (mass displacements—x_{ij} $\{i = 1$ to 20 and $j = 1$ to 20$\}$). The mass displacements for $i = 20$ were held fixed to simulate the fixed grip condition of the frozen tongue specimen and the mass displacements for $i = 1$ were fixed initially (as required by symmetry) and then released as bonds were broken along the crack path.

using a network of 20 elements in height and 20 elements in width. Lines between the masses represent tension (T) springs in the vertical direction and shear (S) springs in the horizontal direction, as annotated in Fig. 2. Viscous damping can be added when required to these elements and across the crack tip. More involved mass, spring, viscous damping networks could be used, but the simple option shown was easily able to provide the required data which compared closely with those obtained from more powerful finite element and other models. In an early model, in addition to the vertical tension (T) and horizontal shear (S) springs, cross-diagonal springs were employed, and each mass had two degrees of freedom in directions normal and parallel to the crack path. This model exhibited the Poisson's contraction effect. However, removing the cross-diagonal springs and confining the masses to one degree of freedom, normal to the crack path, had little effect when determining dynamic energy release rates. Also, in this version of the model, only the values of the tension (T) and the shear (S) springs needed to be changed to represent the Poisson's ratio (ν) of each material to be modelled. These modifications usefully reduced the computational load to a level well within the capability of PCs of modest power and did not introduce unacceptable errors. An advantage of these distributed mass, spring, viscous damping networks is that they fit neatly between Williams lumped constant models [7] and dynamic finite element (FE) models [8–10].

When the distributed mass-spring model is tensioned, normal to the crack path, strain energy is initially stored in the tension (T) springs and the shear (S) springs are unaffected. When the crack is propagating and the masses along the designated crack path are released, there is a transfer of strain energy from the tension (T) springs to the shear (S) springs. PC machines are capable of carrying out step-by-step integration to represent this dynamic strain energy transfer process. This is the process resulting in a build-up of shear strain at, and ahead of, the crack tip. The rate and extent of the redistribution and build-up of strain at the crack tip is thus determined by the response characteristics of the distributed mass-spring network. It follows that the faster the crack bonds are broken, the less time there is for the network to affect the conversion of tensile strain energy (T springs) to shear strain energy (S springs) and to transfer strain energy to the advancing crack tip. The Poisson ratio of the material to be represented is used to determine the relative stiffness of the T and S springs. Similarly, the PC model's mass, distributed viscous damping and energy absorbing elements at the crack tip are related to the material to be simulated. Equations of motion for each mass in the modelling network provide a basis for a step-by-step programme to compute the motion of the sprung masses as the crack moves along a designated path. For the model shown in Fig. 2, these equations are as follows:

$$\begin{aligned} m\frac{\mathrm{d}^2x_{ij}}{\mathrm{d}t^2} &= -k_T[x_{ij} - x_{(i+1)j}] - k_T[x_{ij} - x_{(i-1)j}] \\ &\quad - k_S[x_{ij} - x_{i(j+1)}] - k_S[x_{ij} - x_{i(j-1)}] \\ &\quad - \eta_T\left[\frac{\mathrm{d}x_{ij}}{\mathrm{d}t} - \frac{\mathrm{d}x_{(i+1)j}}{\mathrm{d}t}\right] - \eta_T\left[\frac{\mathrm{d}x_{ij}}{\mathrm{d}t} - \frac{\mathrm{d}x_{(i-1)j}}{\mathrm{d}t}\right] \\ &\quad - \eta_S\left[\frac{\mathrm{d}x_{ij}}{\mathrm{d}t} - \frac{\mathrm{d}x_{i(j+1)}}{\mathrm{d}t}\right] - \eta_S\left[\frac{\mathrm{d}x_{ij}}{\mathrm{d}t} - \frac{\mathrm{d}x_{i(j-1)}}{\mathrm{d}t}\right] \end{aligned} \quad (1)$$

where the displacement of each mass (m) is x_{ij} in a direction normal to the crack path and the stiffness and damping of the tension (T) and shear (S) springs are k_T, η_T and k_S, η_S, respectively. Each element in the model would need to relate to the size and properties of a corresponding element in a real material, and the following factors in particular

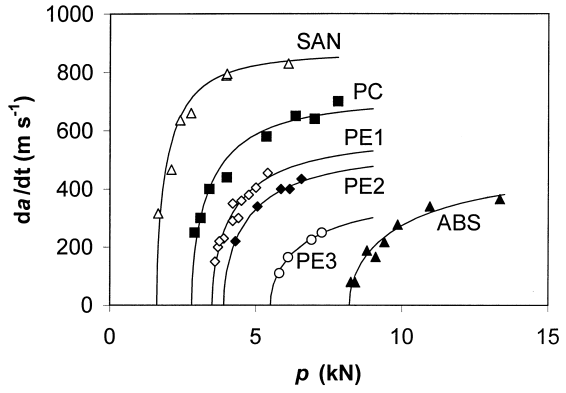

Fig. 3. Crack velocity, da/dt, versus load, p, at crack initiation for frozen tongue experiments on SAN(△), PC(■), PE1(◇), PE2(◆), PE3(○) and ABS(▲). A curve (given by Eq. (4)) is fitted through each set of frozen tongue data to obtain values for p_0 and C_L (given in Table 1).

need to be taken into account:

$$m = \rho B L^2, \qquad C_0 = L\sqrt{\frac{k_T}{m}}, \qquad k_T = EB,$$
$$k_S = \frac{EB}{2(1+\nu)}, \quad \eta_T = 2\xi_T\sqrt{k_T m}, \quad \eta_S = 2\xi_S\sqrt{k_S m} \tag{2}$$

where ρ is density, E is the Young's modulus, C_0 is the longitudinal wave velocity (equal to $(E/\rho)^{1/2}$), ν is Poisson's ratio, B is thickness, L is spacing of masses and ξ_T and ξ_S are non-dimensional damping ratios for the T and S springs. The use of $C_0 = (E/\rho)^{1/2}$ is appropriate for the model because the masses only have one degree of freedom in the direction normal to the crack path. When making specific comparisons between different materials but identically shaped specimens, the equations can be simplified by normalisation. A modelling point is that care is needed in selecting a suitably small time-step to reduce the build-up of computational error, particularly when the transient behaviour of the structure is complex.

The crack tip conditions can be modelled in several ways, but the version used here was the same as that often employed in FE networks [8,9]. One feature is to provide an energy sink and a smooth opening of the crack tip by applying a decaying hold-back force to each crack path mass as its bond is broken. The other feature is to reduce the modulus of the elements immediately adjacent to the crack path using reduced stiffness for the T and S springs (k_T and k_S). These two features represent the toughness of the material or the energy absorbed at the crack tip, and also the change in material properties in the crack tip zone. This includes the effects of yielding, crazing, micro-cracking, drawing of fibrils, the generation of a hot-spot and other energy absorbing processes in the zone about the crack tip.

The dynamic energy release rate, G_{dyn}, is given by:

$$G_{dyn} = \frac{1}{B}\left[\frac{dU_e}{da} - \frac{dU_s}{da} - \frac{dU_k}{da} - \frac{dU_d}{da}\right] \tag{3}$$

where B is thickness, a is crack length, U_e is external work done, U_s is the stored strain energy, U_k is kinetic energy and U_d is the dissipated energy in the distributed viscous damping elements. G_{dyn} can also be obtained from the distributed mass-spring model as the work done against the hold-back force which resists the opening of the crack. For this study, the generation mode was employed to obtain dynamic energy release rates (G_{dyn}) for many different crack velocities.

4. Results

Fig. 3 shows the crack velocity (da/dt) versus load (p) curves for the fracture of all the materials researched in this study. For each of the different materials, a curve is fitted through the plotted frozen tongue data of the form:

$$\frac{da}{dt} = C_L\left[1 - \left(\frac{p_0}{p}\right)^2\right]^{1/2} \tag{4}$$

where C_L is limiting crack velocity and p_0 is the threshold value of load for crack propagation. The fitting procedure provides a good measure of p_0 and C_L for each material. The Young's modulus, E, and Poisson's ratio, ν, for each material were determined using longitudinal and transverse wave velocity measurements for an excitation frequency of 2 MHz. The density, ρ, for each material was from manufacturers' verified data. The values of p_0, C_L, E, ν and ρ for each material are given in Table 1. From these data, the longitudinal wave velocity ($C_0 = (E/\rho)^{1/2}$) and the limiting crack velocity normalised by the longitudinal wave velocity (C_L/C_0) are evaluated.

Table 1
Data for threshold load (p_0) and limiting crack velocity (C_L) from frozen tongue experiments, Young's modulus of the bulk material (E) and Poisson's ratio (ν) from wave velocity measurements, density (ρ) from manufacturers' verified data. Also, shown are the longitudinal wave velocity ($C_0 = (E/\rho)^{1/2}$) and the limiting crack velocity normalised by longitudinal wave velocity (C_L/C_0)

Material	p_0 (kN)	C_L (m s^{-1})	E (GN m^{-2})	ν	ρ (kg m^{-3})	C_0 (m s^{-1})	C_L/C_0
SAN	1.6	870	3.3	0.36	1060	1760	0.49
PC	2.8	710	3.0	0.38	1190	1590	0.45
PE1	3.5	580	1.9	0.40	945	1420	0.41
PE2	3.9	530	2.1	0.40	951	1490	0.36
PE3	5.5	380	2.3	0.40	954	1550	0.24
ABS	8.2	495	2.7	0.39	1040	1610	0.31

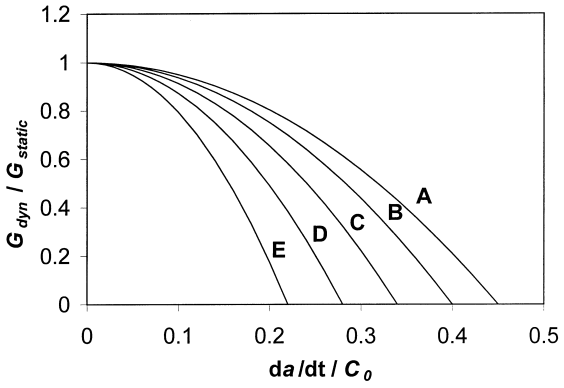

Fig. 4. Normalised dynamic energy release rate (G_{dyn}/G_{static}) versus normalised crack velocity ($da/dt/C_0$) from the distributed mass spring model. Curve A is for $\nu = 0.35$ and $E_{cp}/E = 1$, Curve B is for $\nu = 0.4$ and $E_{cp}/E = 1$, Curve C is for $\nu = 0.4$ and $E_{cp}/E = 0.5$, Curve D is for $\nu = 0.4$ and $E_{cp}/E = 0.25$ and Curve E is for $\nu = 0.4$ and $E_{cp}/E = 0.125$ (where E_{cp} is the Young's modulus of the elements immediately adjacent to the crack path and E is the Young's modulus of the bulk material).

Fig. 4 shows a set of curves for normalised dynamic energy release rate (G_{dyn}/G_{static}) versus normalised crack velocity ($da/dt/C_0$) obtained from the distributed mass-spring model functioning in the generation mode. The value of G_{static} relates to a very slowly propagating crack. It is to be noted that as the crack velocity is increased, the dynamic strain energy available to the crack tip (G_{dyn}) reduces at an increasing rate. The point on each curve, which intersects the horizontal axis, gives the maximum or limiting crack velocity (C_L/C_0). Curve A relates to a material with a Poisson's ratio (ν) of 0.35 and no reduction in modulus of the elements immediately adjacent to the crack path ($E_{cp}/E = 1$ where E_{cp} is the crack path Young's modulus and E is the Young's modulus of the bulk material). Curve B is for a Poisson's ratio (ν) of 0.4 and no reduction in modulus of the elements immediately adjacent to the crack path ($E_{cp}/E = 1$). Curve C is for $\nu = 0.4$ and $E_{cp}/E = 0.5$, Curve D is for $\nu = 0.4$ and $E_{cp}/E = 0.25$ and Curve E is for $\nu = 0.4$ and $E_{cp}/E = 0.125$. For curves

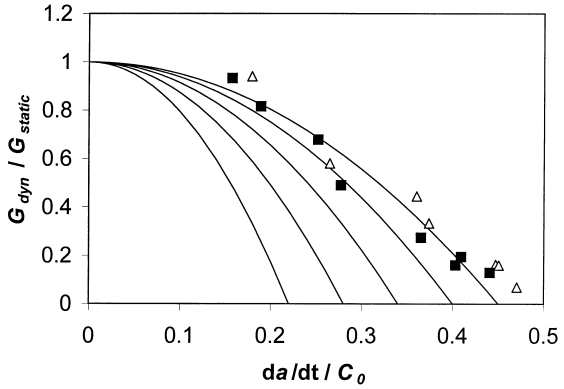

Fig. 5. Normalised dynamic energy release rate (G_{dyn}/G_{static}) versus normalised crack velocity ($da/dt/C_0$) distributed mass-spring model curves together with frozen tongue data for SAN(△) and PC(■).

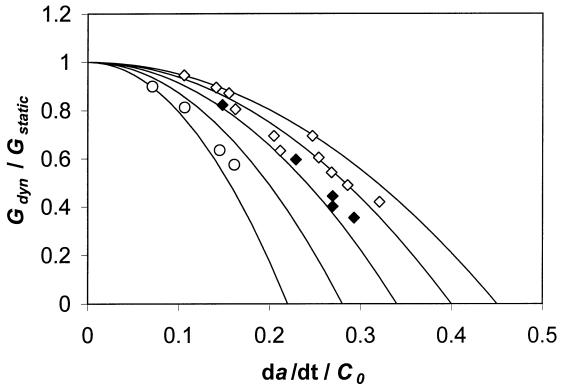

Fig. 6. Normalised dynamic energy release rate (G_{dyn}/G_{static}) versus normalised crack velocity ($da/dt/C_0$) distributed mass-spring model curves together with frozen tongue data for PE1(◇), PE2(◆) and PE3(○).

C–E, the reduction in crack path modulus (E_{cp}) was achieved by reducing the stiffness of the model's springs (k_T and k_S), immediately adjacent to the crack path, to increase the toughness of the zone about the crack tip. The model data in Fig. 4 shows that this leads to a reduction in limiting crack velocity (C_L). Also shown in Fig. 4, the limiting crack velocity (C_L) is altered by a change in the Poisson's ratio (ν). It is to be noted that the Poisson's ratio (ν), for the polymers studied here, only ranges from 0.36 (SAN) to 0.4 (PE1, PE2 and PE3). In the model, the Poisson's ratio determines the relative stiffness of the T and S springs (k_T and k_S).

The frozen tongue experimental data can be compared with data from the distributed mass-spring model (as shown in Fig. 4) by using the following relationship:

$$\frac{G_{dyn}}{G_{static}} = \left(\frac{p_0}{p}\right)^2 \tag{5}$$

where p is the load on the frozen tongue specimen and p_0 is the threshold value of load for crack propagation in each material. This is based on the Griffith relationship that G_{static} varies as p^2a/E where p is the load on the specimen, a is the crack length and E is the Young's modulus of the bulk material. Also, G_{dyn} varies as p_0^2a/E where p_0 is the threshold load to just sustain crack propagation since G_{dyn} is equal to the fracture resistance of the material.

Fig. 5 shows normalised dynamic energy release rate (G_{dyn}/G_{static}) versus normalised crack velocity ($da/dt/C_0$) distributed mass-spring model curves, together with frozen tongue data for SAN(△) and PC(■). The data for SAN ($\nu = 0.36$) is appropriately near the model's curve A for $\nu = 0.35$ with a limiting crack velocity (C_L) of 0.45 C_0 and the data for PC ($\nu = 0.38$) is closer to the model's curve B for $\nu = 0.4$ with a limiting crack velocity (C_L) of 0.4 C_0.

Fig. 6 shows normalised dynamic energy release rate (G_{dyn}/G_{static}) versus normalised crack velocity ($da/dt/C_0$) distributed mass-spring model curves, together with frozen tongue data for three grades of polyethylene of increasing

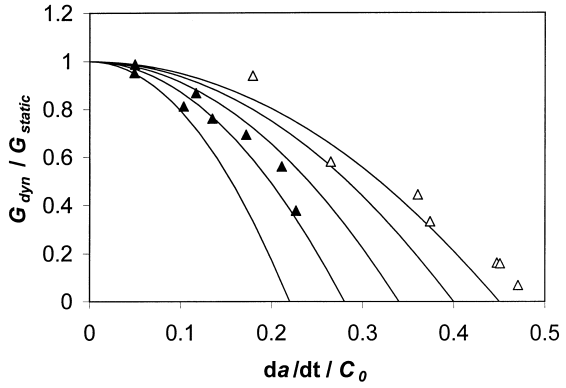

Fig. 7. Normalised dynamic energy release rate (G_{dyn}/G_{static}) versus normalised crack velocity ($da/dt/C_0$) distributed mass-spring model curves together with frozen tongue data for SAN(△) and ABS(▲).

toughness (PE1-◇, PE2-◆ and PE3-○). Data for the PE1 ($\nu = 0.4$) is mostly on the model's curve B for $\nu = 0.4$ with a limiting crack velocity (C_L) of 0.4 C_0. The data for PE2 ($\nu = 0.4$) is nearer the model's curve C for $\nu = 0.4$ with a limiting crack velocity (C_L) of 0.34 C_0. The data for PE3 ($\nu = 0.4$) is nearer the model's curve E for $\nu = 0.4$ with a limiting crack velocity (C_L) of 0.22 C_0. The model's curves C–E are for increasing toughness in the crack tip zone. This is achieved by reducing their crack path modulus (E_{cp}), namely $E_{cp}/E = 0.5$ for curve C, $E_{cp}/E = 0.25$ for curve D and $E_{cp}/E = 0.125$ for curve E.

Fig. 7 shows normalised dynamic energy release rate (G_{dyn}/G_{static}) versus normalised crack velocity ($da/dt/C_0$) distributed mass-spring model curves, together with frozen tongue data for SAN(△) and ABS(▲). This ABS material has a SAN matrix filled with 30% by volume of rubber particles of a size 0.1–0.2 μm. The SAN material is near to the model's curve A and the ABS material is centred on the model's curve D. It is evident that there is a marked reduction of the limiting crack velocity (C_L/C_0) which relates to the toughening effect of the rubber particles. It is to be noted that the bulk value of Young's modulus of ABS (2.7 GN m^{-2}) is only a little less than that of SAN (3.3 GN m^{-2}) and their longitudinal wave velocities (C_0) are not greatly different. The main toughness effect of the ABS rubber particles is within the crack tip zone which relates to the reduction in crack path modulus used in the distributed mass-spring model to represent ABS and other tough materials.

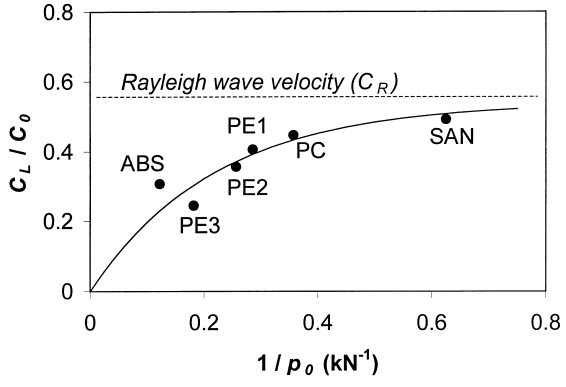

Fig. 8. Plot of C_L/C_0 versus $1/p_0$ for all six materials evaluated with the frozen tongue technique. The tougher the polymer (high p_0), the greater the difference between the limiting crack velocity (C_L) and its Rayleigh surface wave velocity (C_R).

Fig. 8 is a plot of C_L/C_0 versus $1/p_0$ for all six materials evaluated with the frozen tongue technique. This shows that the tougher the polymer (higher p_0), the greater the difference between the limiting crack velocity (C_L) and its Rayleigh surface wave velocity (C_R which is $\sim 0.57C_0$ when $\nu = 0.36$). Again, in evidence is the marked reduction of C_L/C_0 of ABS with respect to SAN the matrix material.

5. Discussion

The main findings and observations are as follows:

- The tougher the polymer, the lower the limiting crack velocity. Only very brittle polymers have a limiting crack velocity (C_L) approaching the Rayleigh surface wave velocity (C_R).
- The energy absorbing fracture processes at and about the crack tip vary from one material to another, particularly for tougher materials, such as ABS.
- The fracture processes at and about the crack tip zone include, for example, yielding, crazing, micro-cracking, as well as fibril and other drawing of material from the fracture surfaces. These processes can also raise the temperature of the material in the crack tip zone. Overall, the dynamic effects of these crack tip zone processes can effectively be modelled by using a zone about the crack path of reduced modulus.
- The effect of energy absorbing fracture processes, in the zone about the crack tip, including the resultant lowering of the modulus of the material in the crack path zone, reduces the dynamic rate of strain energy transfer to the crack tip.
- The size of the frozen tongue specimens used was large enough to avoid boundary effects unduly limiting the region around the crack tip from which strain energy is dynamically transferred to the crack tip. The crack velocity versus applied load curves, therefore, readily represent the fracture behaviour of the range of polymer materials studied.
- The crack velocity versus load curve for ABS in Fig. 3 differs from the curves for homogeneous polymers (SAN, PC and the three grades of PE) in the relationship between the threshold load (p_0) and the limiting crack velocity (C_L). This is because the toughening effect of rubber particles in the ABS varies with crack velocity.
- The toughness effect of the rubber particles in the SAN host material of ABS is considerable as can be seen by comparing the SAN and ABS curves in Figs. 3 and 7.

Notably, there is a greater increase of the threshold load (p_0) but less of a reduction of the limiting crack velocity (C_L) by the rubber particles in ABS.

- The evaluation procedures used in this study, examining mostly homogeneous polymers, can also be usefully employed to research polymers that have non-linear characteristics to identify, for example, toughening techniques.
- The distributed mass-spring model was easily able to simulate the dynamic strain energy release rate (G_{dyn}/G_{static}) versus crack velocity ($da/dt/C_0$) characteristics of polymers. This included representing the crack tip zone processes that increased the toughness of the material, and the reduction of the region about the crack tip, with increasing crack velocity, which is able to provide strain energy to the crack tip.
- The ability to represent the crack tip zone effects, by varying the crack path modulus (E_{cp}), in the distributed mass-spring model, allowed the limiting crack velocity (C_L) behaviour of different materials to be simulated. Also, the effect of Poisson's ratio (ν) on the limiting crack velocity (C_L) could be examined by the distributed mass-spring model.

6. Conclusions

Yielding, crazing and other processes change the material properties about the crack tip. It was possible to simulate this effect in the distributed mass-spring model by reducing the stiffness of the model's elements immediately adjacent to the crack path. This had the appropriate effect of increasing the toughness and reducing the rate at which strain energy could be transferred, within the crack tip zone, to the crack tip. For tough materials, this is a significant factor in explaining the relationship between limiting crack velocity and toughness.

In addition to the specific findings summarised above, the experimental and modelling data obtained relates to other factors. For instance, for more brittle polymers the loading level above the threshold load (p_0) which will produce a limiting crack velocity (C_L) is quite small, with the result that the impact of brittle polymers often results in cracks propagating away from the impact site near to the limiting crack velocity. Also, there is often sufficient impact energy to propagate several cracks at high velocity so as to shatter the material. Other brittle materials, including glass and ceramics, have similar impact fracture characteristics to those of very brittle polymers.

Acknowledgements

The author thanks the Engineering and Physical Sciences Research Council (EPSRC), the Polymer Engineering Group (PEG), BP Chemicals and Monsanto for their valuable help and support as well as provision of materials.

References

[1] Dear JP. J Mat Sci 1991;26:321.
[2] Dear JP, Williams JG. J Mat Sci 1993;28:259.
[3] Dear JP. J Mat Sci 1995;30:2485.
[4] Rosakis AJ, Samudrala O, Coker D. Science 1999;284:1337.
[5] Field JE. Cont Phys 1971;12(1):1.
[6] Washabaugh PD, Knauss WG. Int J Fract 1994;65:97.
[7] Williams JG. Int J Fract 1987;33:47.
[8] Ivankovic A, Williams JG. Int J Fract 1993;64:251.
[9] Keegstra PNR, Head JL, Turner CE. In: Taplin DMR, editor. Proceedings of the Fourth International Conference on Fracture, Waterloo, Paper 346, 1977.
[10] Nishioka T, Atluri SN. J App Mech 1980;47:570.